

# Structurally Induced Large Changes of the Energy Level Alignment in CuPc on Cu(110)-(2x1)O

B. Maughan, P. Zahl

To be published in "Physical Review B"

October 2018

Center for Functional Nanomaterials  
**Brookhaven National Laboratory**

**U.S. Department of Energy**  
USDOE Office of Science (SC), Basic Energy Sciences (BES) (SC-22)

Notice: This manuscript has been authored by employees of Brookhaven Science Associates, LLC under Contract No. DE-SC0012704 with the U.S. Department of Energy. The publisher by accepting the manuscript for publication acknowledges that the United States Government retains a non-exclusive, paid-up, irrevocable, world-wide license to publish or reproduce the published form of this manuscript, or allow others to do so, for United States Government purposes.

## **DISCLAIMER**

This report was prepared as an account of work sponsored by an agency of the United States Government. Neither the United States Government nor any agency thereof, nor any of their employees, nor any of their contractors, subcontractors, or their employees, makes any warranty, express or implied, or assumes any legal liability or responsibility for the accuracy, completeness, or any third party's use or the results of such use of any information, apparatus, product, or process disclosed, or represents that its use would not infringe privately owned rights. Reference herein to any specific commercial product, process, or service by trade name, trademark, manufacturer, or otherwise, does not necessarily constitute or imply its endorsement, recommendation, or favoring by the United States Government or any agency thereof or its contractors or subcontractors. The views and opinions of authors expressed herein do not necessarily state or reflect those of the United States Government or any agency thereof.

# Structurally Induced Large Changes of the Energy Level Alignment in CuPc on Cu(110)-(2x1)O

*Bret Maughan,<sup>1</sup> Calley N. Eads,<sup>1</sup> Percy Zahl,<sup>2</sup> and Oliver L. A. Monti<sup>1,3\*</sup>*

<sup>1</sup>University of Arizona, Department of Chemistry & Biochemistry, 1306 E. University Blvd.,  
Tucson, AZ 85721, USA

<sup>2</sup>Brookhaven National Laboratory, Center for Functional Nanomaterials  
Upton, NY 11973, USA

<sup>3</sup>University of Arizona, Department of Physics, 1118 E. Fourth Street, Tucson, AZ 85721, USA

e-mail address: [monti@u.arizona.edu](mailto:monti@u.arizona.edu)

KEYWORDS CuPc, Cu(110), STM, UPS, Energy level alignment, thin film structure

**Abstract**

Though it is becoming apparent that organic semiconductor / metal interfaces may exhibit a variety of different structural phases, it is at present unclear to what extent these different thin film structures determine the interfacial electronic structure. Here, we observe for the case of copper(II) phthalocyanine (CuPc) on Cu(110)-O(2x1) large changes in the interfacial electronic structure beyond the first monolayer of CuPc, particularly evident in the frontier orbital region. Using scanning tunneling microscopy in conjunction with photoemission spectroscopy, we characterize the ultrathin-films of CuPc grown on oxygen reconstructed Cu(110) and propose that the unique changes to the electronic structure are the result of an abrupt transition in film structure between the first and second layers. Specifically, an interface layer of ordered, flat-lying molecules templates a largely vertical, standing-up orientation of molecules in the subsequent layer. The anisotropic charge distribution of the molecule accounts for the sizeable and unusual change in ionization energy between molecules in the two layers. Our results demonstrate that the precise structure of the organic semiconductor film may exert an important role in determining the interfacial electronic structure that may be harnessed to tailor energy level alignment at such interfaces.

## Introduction

One of the consistent motivations for studying organic semiconductors and their interfaces is the desire to discover new materials and materials combinations that improve on the functionality, power, and efficiency of modern electronic devices.<sup>1-3</sup> Progress in both theoretical and experimental capabilities has propelled the field rapidly in recent years and, as a result, molecular-based devices are currently enhancing traditional semiconductor devices in commercial optoelectronic applications such as e.g., photovoltaic and visual display technologies.<sup>4</sup> Organic semiconductors hold additional value as promising components in next-generation device applications where shrinking device scale, biocompatibility, and mechanical flexibility are primary objectives.

Central to efforts for tailoring device properties has been the recognition that the interfaces between the organic semiconductor and e.g. the metal contacts may determine device function and efficiency. As the result of advances made both in experiment and theory, there are by now a range of models that offer a certain level of explanatory power of the electronic structure of specific types of interfaces.<sup>5-10</sup> Molecular self-assembly and the structure of the organic semiconductor film is implicitly and sometimes explicitly a key ingredient in all of these models. This is important, since organic thin films may exhibit a plethora of different phases and structures over often a small temperature and coverage range, and one may expect as a result different interfacial electronic structures associated with each thin film phase.<sup>11-13</sup> The scientific challenge derives then from a need to understand *how* these different thin film structures influence the interfacial electronic structure, and in turn to what extent thin film structure, perhaps extended to multicomponent systems,<sup>4</sup> may be ultimately tailored to enhance desirable device properties.

Clearly, a combination of methods that provide structure and energy levels is necessary to achieve this goal.

Some insight into this question may be gained from varying the nature of the organic semiconductor,<sup>14</sup> the substrate crystal face on which the film is grown,<sup>15</sup> or from introducing interlayers.<sup>16,17</sup> These methods draw strength from the rich diversity of available molecular platforms and the specific interactions with distinct surfaces, but require a comparison across inherently different interfaces. In contrast, structural transitions and associated control of the interfacial electronic structure for a single specific organic / metal interface are much rarer,<sup>11-13,18</sup> but offer an important and internally consistent step towards a deeper understanding of the forces that control interfacial electronic structure and energy level alignment. This has the advantage of observing molecular-level structural changes while preserving both the bulk metallic electronic structure and the chemical nature of the molecular film.

Here, we study the CuPc / Cu(110)-(2x1)O interface as an example of a system where a surprisingly large change in the interfacial electronic structure is observed near a coverage of 1 monolayer. Based on a combination of scanning tunneling microscopy (STM) and angle-resolved photoemission spectroscopy (ARPES), we propose to attribute this change to a structural transition from face-on flat-lying CuPc molecules up to 1 monolayer to a standing molecular orientation at coverages beyond 1 monolayer. This structural richness is in contrast to CuPc on Cu(110) and most organic / metal interfaces, where face-on growth over some monolayers with eventual adoption of the bulk organic crystal structure is the norm.<sup>16,19-21</sup> It is enabled by the much weaker surface-molecule interactions enabled by the oxygen chemisorption on Cu(110). The fact that such a structural transition is observed within a single organic / metal interfacial system permits us to interpret the large changes in the interfacial electronic structure based on simple electrostatic

arguments and provides an avenue for realizing large energy level offsets at organic semiconductor interfaces.

## Methods

Copper Phthalocyanine (CuPc, Sigma-Aldrich / 95%) was purified by triple sublimation in a custom-built vacuum furnace ( $5 \times 10^{-7}$  torr). The Cu(110) crystal (Princeton Scientific) was cleaned by repeated cycles of Ar<sup>+</sup> sputtering (1-2 keV, 5-10  $\mu\text{A}/\text{cm}^2$ ) and annealing (850 K). Cleanliness was verified directly in STM images or by the work function ( $\Phi = 4.6(1)$  eV) in ultraviolet photoemission spectroscopy (UPS). The Cu(110)-(2x1)O surface was prepared by backfilling the vacuum chamber with O<sub>2</sub> at low pressure ( $p \sim 3.0 \times 10^{-8}$  torr) to ensure growth of the (2x1) reconstruction. Exposures are expressed in Langmuirs (1L =  $10^{-6}$  torr · s). Thin-films of CuPc were evaporated onto room temperature Cu(110)-(2x1)O using a home-built, water-cooled Knudsen source in a sample preparation chamber (base pressure of  $< 1 \times 10^{-9}$  torr). Films were grown at a typical rate of 0.1 monolayer/min, as monitored by quartz crystal microbalance. Film thickness is reported as a fraction of a hypothetical closed monolayer (ML) of flat-lying molecules (1 ML  $\approx 4.44 \times 10^{13}$  molecules/cm<sup>2</sup>) and referred to as nominal thickness.

For STM, the sample was transferred to the imaging chamber (pressure  $< 10^{-11}$  torr) immediately following sample preparation, where it remained at room temperature for 2 min before rapid quenching to 77 K and continued cooling to 5 K. All STM images were acquired at 5 K, with the instrument in constant current mode, and using an electrochemically etched PtIr tip. Microscope control and image processing were performed using the GXSM software package.<sup>22</sup> All photoemission experiments (analysis chamber pressure  $< 10^{-10}$  torr) were performed at room temperature with an unpolarized Scientific Instruments UVS 200 He lamp. The energy resolution

of the analyzer is approximately 70 meV as determined by Fermi level broadening of the clean surface. Work functions were determined from spectra taken with a -5 V bias to facilitate analysis of the secondary cutoff edge. For angle-resolved experiments (ARPES), the bias was reduced to -3 V and the electron acceptance angle narrowed to  $\pm 1.5^\circ$ . Crystal azimuthal orientation with respect to the surface Brillouin zone was determined using low energy electron diffraction (LEED) with an estimated angle accuracy of  $\pm 5^\circ$ .

## Results

### Interfacial electronic structure

Normal emission UPS data for nominal coverages of CuPc on oxidized Cu(110) are shown in Figure 1. Prior to molecular deposition, the surface was prepared by exposure of clean Cu(110) to  $\sim 24$  L O<sub>2</sub> at 100 °C. This procedure results in a surface fully saturated with the oxygen-induced  $p(2 \times 1)$  reconstruction (Cu(110)-(2x1)O).<sup>23,24</sup> Molecular contributions to the electronic density of states (DOS) are evident with increasing nominal CuPc coverage in the spectral sequence of Figure 1a: Data for thicker films show very clearly the emergence of molecular features in several regions below the intense Cu(110) d-bands and near the Fermi level ( $E_F$ ) at binding energies ( $E_F - E$ ) of around -1 eV. The system does not exhibit any distinct molecular feature at  $E_F$ , which would have indicated interfacial charge-transfer, and is commonly encountered in strongly hybridized interfaces.<sup>17,25-27</sup> The accompanying work function changes  $\Delta\Phi$  are also shown in Figure 1a (inset), plotted relative to pristine Cu(110)-(2x1)O ( $\Phi = 4.9(1)$  eV). The work function decreases monotonically with increasing coverage to give  $\Delta\Phi = -0.54$  eV at a nominal film thickness of 4 ML. For the first monolayer of CuPc,  $\Delta\Phi$  of  $\sim -0.32$  eV is comparable to titanyl phthalocyanine on bare Cu(110),<sup>26</sup> indicating that pushback of the surface electronic wave function is significant even for the oxidized surface.

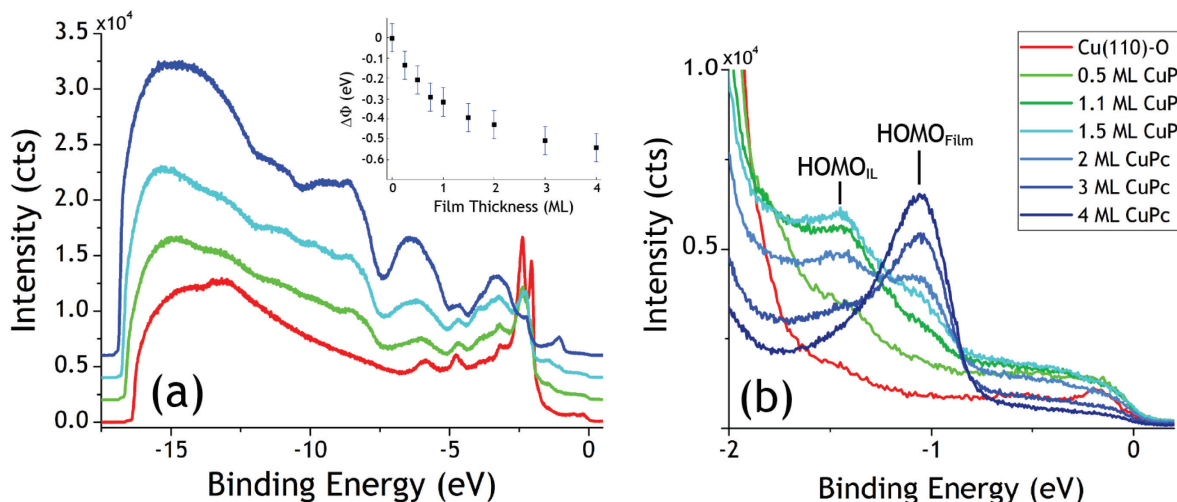


Figure 1. (a) Normal emission UPS spectral sequence for thin-film growth of CuPc on Cu(110)-(2x1)O. Spectra offset for clarity. Inset: Plot of work function change ( $\Delta\Phi$ ) as a function of nominal film thickness. (b) Frontier orbital region evolution as a function of nominal CuPc coverage. The legend indicates nominal coverage in both panels (a) and (b).

Focusing our attention on the frontier orbital region near  $E_F$ , a molecular feature at -1.4 eV binding energy develops at low coverages (see e.g. 0.5 ML spectrum in Figure 1b). This is the HOMO of molecules forming the interfacial layer which are in direct contact with the surface. We refer to this layer henceforth as the interface layer (IL). STM data supporting this assignment are discussed in detail below (see Figure 3). The  $\text{HOMO}_{\text{IL}}$  intensity increases with coverage until a maximum is reached between 1 and 1.5 ML, whereafter its intensity decreases. Meanwhile, an additional molecular feature at -1 eV appears at coverages near a nominally full monolayer and continues to grow with increasing coverage. Due to the behavior of this feature as a function of molecular coverage, we attribute it to the HOMO of molecules in the second layer and beyond, and label it  $\text{HOMO}_{\text{Film}}$ .

The relative binding energies of these two HOMOs are somewhat unusual for three salient reasons: First, the fact that the  $\text{HOMO}_{\text{IL}}$  binding energy is *larger* than that of the  $\text{HOMO}_{\text{Film}}$  is not commensurate with simple considerations of work function change ( $\Delta\Phi$ ) and interface dipoles; if

both features had a common electronic origin, HOMO<sub>IL</sub> would be expected to appear at a *lower* binding energy as the work function drops with coverage (Figure 1a inset),<sup>28,29</sup> contrary to our findings. This indicates that the two spectroscopic features report on electronically different CuPc species in the first few layers. Further, this observation indicates that interactions beyond simple interface dipoles are significantly shaping the interfacial electronic structure. Second, when accounting for  $\Delta\Phi$ , the ionization energy of first layer molecules is much greater than that of second layer molecules (5.4 eV vs. 6 eV), at odds with a simple polarization energy picture.<sup>30,31</sup> Third, the dramatic change in ionization energy occurs *abruptly* with the growth of the second layer of molecules, instead of evolving gradually as the film grows.<sup>19</sup> Importantly, these observations contrast with the electronic structure of CuPc on other surfaces,<sup>32–37</sup> and instances where multiple HOMOs have been observed in phthalocyanine films.<sup>38,39</sup> Together, they point to an abrupt structural transition once the second layer is forming.

To understand the underlying causes for the interface evolution, we consider each of these points in more detail in what follows, aided by a closer analysis of the region near  $E_F$ . Figure 2a shows a fit with a single Gaussian (linear background) for each of the two HOMO features in the nominally 1.5 ML film. The HOMO<sub>IL</sub> HWHM (191(8) meV) is significantly wider than the HOMO<sub>Film</sub> HWHM (98(5) meV), an indication of some degree of coupling with the surface. The possible role of inhomogeneous broadening and substantial structural disorder in the interface layer is minor, as is evident from the STM data (see below). The HOMO<sub>IL</sub> and HOMO<sub>Film</sub> are centered at -1.469(3) and -1.096(3) eV binding energy, respectively, a difference of 373 meV. An HOMO<sub>IL</sub> ionization energy much greater than that of the HOMO<sub>Film</sub> excludes electronic polarization effects at the interface as the source of the two molecular features.<sup>30,40,41</sup> Additionally, not only is the *order* of HOMO energies in contradiction to expectations for photohole screening,

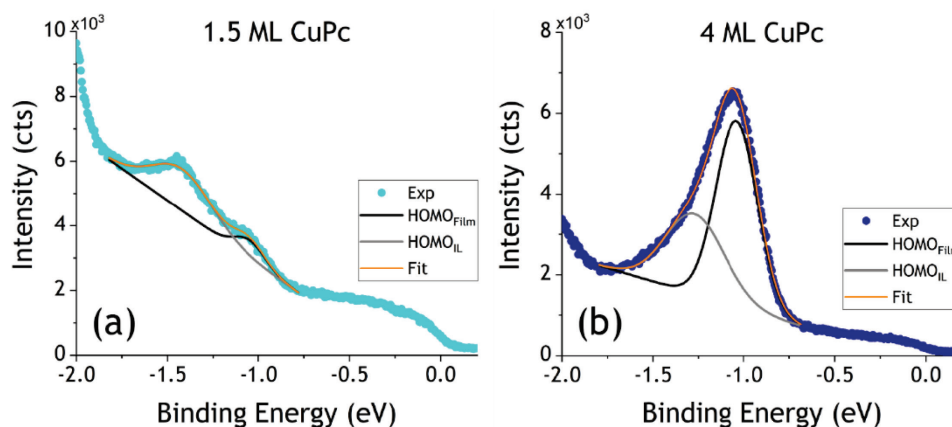


Figure 2. (a) Fit of the HOMO<sub>IL</sub> and HOMO<sub>Film</sub> in a 1.5 ML thick film. (b) Fit of HOMO<sub>IL</sub> and HOMO<sub>Film</sub> in a 4 ML thick film.

but the *magnitude* of the energy difference is also significantly larger than typically observed between interface layer and the next few molecular layers, as seen e.g. in 1-2 ML CuPc on HOPG,<sup>36</sup> and other organic semiconductors on various surfaces.<sup>30,42–47</sup> The magnitude is greater even than suggested “band bending” effects in tens of layers of CuPc on HOPG,<sup>33,48</sup> Si(111),<sup>32,37</sup> Au(100),<sup>34</sup> and Au(110).<sup>40</sup> Thus both the orbital ordering and separation show convincingly that the difference between the HOMO<sub>IL</sub> and HOMO<sub>Film</sub> stems from factors beyond mere polarization effects.

Figure 2b shows a fit to the HOMO region of the nominally 4 ML film, again with two Gaussian functions. We do not constrain the peak positions to coincide with those at lower coverages because of changes to the polarization energy for the thicker films,<sup>49</sup> and potential interactions between the two layers. With this model, we find that the HOMO<sub>IL</sub> is located at -1.321 (5) eV and the HOMO<sub>Film</sub> is located at -1.090(2) eV. The ionization energy of the HOMO<sub>IL</sub> has decreased, presumably due to photohole screening effects by the molecular overlayer, and the binding energy difference between the two HOMOs has decreased to 230 meV. Surprisingly, HOMO<sub>IL</sub> is still clearly discernible, and rather intense even, in a film of nominally 4 ML thickness despite the limited escape depth for photoelectrons at this kinetic energy. This is a clear indication

that the growth of CuPc on Cu(110)-O(2x1) is not simply layer-by-layer but might be attributed to island growth or instead involve a more complex structural transition.

To analyze the growth and to understand the unique behavior of the two HOMO features better, we used STM to study the structural properties of the film. Figure 3a shows an STM image for a nominal coverage of 0.9 ML CuPc ( $\sim 80\%$  of terrace area covered) grown on a surface nearly saturated with the Cu(110)-(2x1)O reconstruction (prepared by exposure of Cu(110) at 100 °C to  $\sim 6$  L O<sub>2</sub>; complete saturation occurs at  $\approx 7$  L O<sub>2</sub>).<sup>24</sup> Molecules assemble into well-ordered rows directed along [001], leading to the formation of ordered monolayer CuPc islands. Figure 3b provides a detailed view of the molecular arrangement in such islands. Individually, CuPc molecules lie with the molecular plane nearly parallel to the surface as indicated by four fully resolved and almost symmetric ligand lobes. A slight molecular tilt or distortion is evident in that some lobes appear brighter than others. The geometry mismatch of the rectangular Cu(110)-

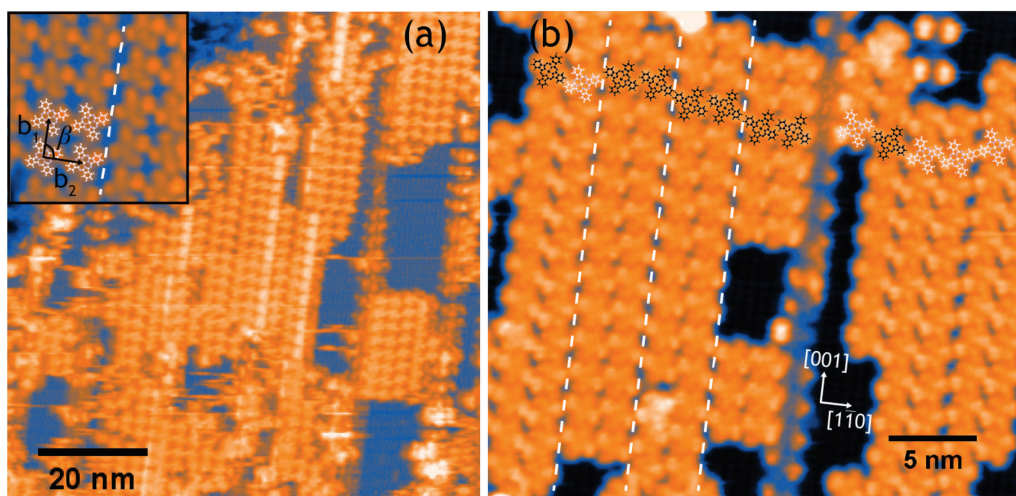


Figure 3. (a) Overview constant current STM image of 0.9 ML CuPc grown on a nearly saturated Cu(110)-(2x1)O surface (Sample bias  $V_s = 100$  mV; tunneling current = 10 pA). Inset: example of molecular detail in ordered islands. (b) Atomically-resolved image showing ordered island structure and underlying Cu(110)-(2x1)O lattice. The two orientation of CuPc molecules are indicated with light and dark molecular models, and white dash lines demarkate grain boundaries between double-row domains.

(2x1)O surface and the four-fold symmetry of CuPc leads to the coexistence of  $n$ -row domains of differing sizes ( $n = 1,2,3$ ) coexisting within islands; 2-row domains are the most ubiquitous, similar to F<sub>16</sub>CuPc on Ag(111).<sup>50</sup> Further, there are two equivalent orientations of CuPc (related by the [001] mirror plane), and domains typically comprise only one orientation; some mixed domains are however also observed (Figure 3b). In 2-row domains with one molecular orientation, molecules form a nearly square network with lattice parameters  $b_1 = 14.1(3)$  Å,  $b_2 = 14.7(4)$  Å, and  $\beta = 91(2)^\circ$  with an azimuthal rotation of  $\theta = 1(1)^\circ$  between  $b_1$  and [001] (Figure 3a inset).<sup>51</sup> STM images of films with coverages exceeding nominal thicknesses of 1 ML could not be observed even at 5 K, likely due to the rather weak intermolecular interactions between different molecular layers.

The observation of ordered monolayer islands contrasts with CuPc and TiOPc films on bare Cu(110). Interactions with surface adatoms on Cu(110) play a key role in both the structure and dynamics of room temperature film formation and lead to amorphous films.<sup>52,20</sup> The oxidized surface, however, captures Cu adatoms by assimilating them into the reconstructed lattice.<sup>53,54</sup> By removing free adatoms and mixing O-character into the surface electronic wavefunction, oxygen chemisorption passivates the reactive Cu(110) surface, thereby allowing for a high degree of order in the film. The weakened surface-molecule interaction is evident also from minor tip instability in the STM experiments, as can be seen from the existence of some noisy regions in Figure 3a. We infer from the staggered arrangement of molecules in islands (Figure 3a inset) that intermolecular interactions include hydrogen-bond-like long-range interactions involving the azan atom and peripheral hydrogen atoms.<sup>55</sup>

Taken together and in light of the photoemission results, the STM data are rather surprising: Even at near-ML coverages, CuPc grows in ordered domains, preferentially covering the surface.

We do not observe evidence of multilayer island growth, but find rather that CuPc forms a true interfacial wetting layer on Cu(110)-(2x1)O at coverages reaching 1 ML. Consequently, the origin of the unusual spectroscopic transition between  $\text{HOMO}_{\text{IL}}$  and  $\text{HOMO}_{\text{Film}}$  cannot be the result of island growth, but must rather lie in a profound structural transition that occurs at film thicknesses beyond 1 ML. We next investigate the nature of this film structure transition in more detail.

### **Structural transition**

A molecular level understanding of the film structure is essential when interpreting the interfacial electronic structure. STM alone is however not enough to understand the structure of the film beyond 1 ML, particularly given the weak interaction between molecules in the second layer and the interfacial layer even when imaging at 5 K. The STM data prove a flat-lying first layer of CuPc, while the direction and magnitude of the HOMO shift suggests an abrupt structural transition in the second layer. Here, we propose that a transition from flat-lying molecules in the interfacial layer to standing molecules in the 2<sup>nd</sup> layer and beyond is the source of the striking evolution of the electronic structure in thin films of CuPc on this surface, in analogy to observations of sexithiophene derivatives on Ag(111).<sup>18</sup> We emphasize that an *ordered* flat-lying seed layer is necessary to template standing growth in the second layer, which can only be achieved on the oxidized surface. This is commensurate with the fact that CuPc has been shown to exhibit various molecular orientations in thin-films depending on the strength and type of surface-molecule interaction: In some systems, CuPc adsorbs flat on the surface and gradually reorients toward the bulk crystalline structure in successive layers,<sup>56</sup> while in others, CuPc adsorbs in a standing orientation in the initial layer.<sup>37</sup> Indeed, a buried 3 nm thick interfacial layer of flat-lying molecules followed by an immediate transition to standing molecules has been previously proposed for CuPc on polycrystalline gold.<sup>57</sup>

Initial evidence for a lying-standing bilayer structure of CuPc on Cu(110)-(2x1)O stems from the atypical HOMO ionization energy change in the second layer (Figure 2 and discussion above). Such a structural transition agrees with all the spectroscopic observations and the STM data. The ionization energy is partly determined by the far field effect of the interface dipole that defines the global vacuum level and work function of the system, but it also depends on the near field effects of the local electronic environment, i.e. the charge distribution within the molecule.<sup>58</sup> This has been shown clearly for the case of strongly polar intramolecular bonds,<sup>59,60</sup> and can be expected to play an important role also when changing molecular orientation. Molecular charge distributions give rise to intrinsic electric fields across a molecule that alter the kinetic energy of the photoelectrons and hence the observed ionization energy:<sup>18</sup> e.g., photoelectrons originating from flat-lying molecules interact with an electron rich  $\pi$ -system charge distribution (increasing ionization energy), while photoelectrons emitted from standing molecules sense primarily the electron deficient hydrogen terminated periphery of the molecule (decreasing ionization energy). Therefore, the lower ionization energy of molecules in the second layer indicates a change in the local charge distribution towards lower electron density, consistent with more vertically oriented CuPc molecules.

More evidence for a lying-to-standing transition comes from the very different angle-dependence of the photoemission intensity for the two HOMO features. The angle-dependence of the photoemission intensity reports directly on the vectorial molecular photoemission matrix element and provides thus insight into the molecular orientation on a surface.<sup>61</sup> In the case of CuPc on Cu(110)-O(2x1), HOMO<sub>IL</sub> and HOMO<sub>Film</sub> have rather different angle-dependence, indicating thus different molecular orientation. This is seen clearly even in the presence of a strongly dispersive surface band feature in the angle-resolved data along  $\bar{\Gamma} - \bar{Y}$  of Figure 4. The HOMO<sub>Film</sub>

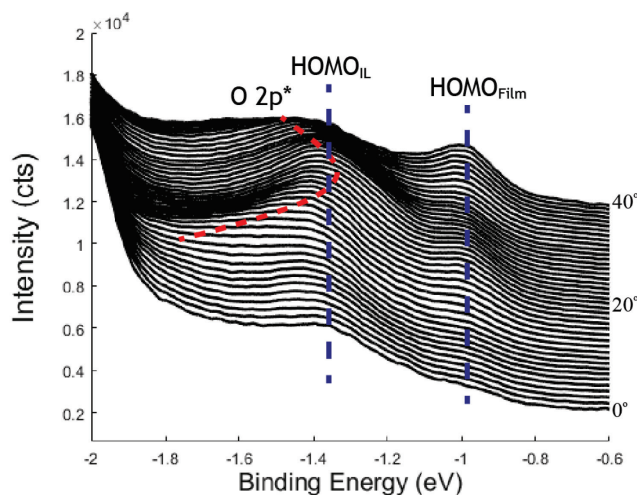


Figure 4. ARPES data of 1.1 ML CuPc film for different polar angles taken along  $\bar{\Gamma} - \bar{Y}$  of the Cu(110)-(2x1)O surface. Antibonding oxygen  $2p$  bands convolute the HOMO<sub>IL</sub> at  $\sim 25^\circ$ , but disperse enough to allow comparison with HOMO<sub>FILM</sub> at  $40^\circ$ .

intensity increases significantly with polar angle, in contrast to the HOMO<sub>IL</sub> (compare e.g. relative intensities at  $0^\circ$  and  $40^\circ$ ). This indicates the existence of different transition dipole moments for molecules in the two layers and is consistent with different molecular orientation in the first and second layer. Along  $\bar{\Gamma} - \bar{X}$  (not shown), interference from a strong Cu(110)  $sp$ -band direct transition<sup>62</sup> obscures the HOMO features, prohibiting assessment as to the specific azimuthal orientation of the standing molecules in the second layer. Nevertheless, both angle-dependence and relative ionization energies suggest that molecules in the second layer orient differently in general, and with the molecular plane more normal to the surface.

The proposed structural transition affects our interpretation of electronic structure measurements when considering the reported film thickness: with the molecular plane oriented largely normal to the surface, the molecule packing density changes dramatically in the second layer. This means that reported (nominal) coverages above 1 ML, based on a hypothetical ML of flat-lying molecules, are in reality much lower: Estimating from crystal structures the separation

between standing molecules to be  $\sim 3.5 \text{ \AA}$ ,<sup>63,64</sup> approximately four times the number of molecules are required to form a full layer of standing molecules. Our nominal 4 ML coverage in Figure 1, established on the assumption of flat-lying layer-by-layer growth, corresponds thus rather to actual 1.75 ML, with the first layer lying flat and the second layer incomplete and consisting of standing molecules. This readily explains the originally puzzling observation of a HOMO<sub>IL</sub> at nominal coverages of 4 ML of flat-lying molecules, a film thickness that exceeds the photoelectron escape depth at these kinetic energies. Instead, partial closure only of the second, standing layer (true coverage of 1.75 ML) leaves 25% of the IL CuPc exposed, responsible for the observed HOMO<sub>IL</sub>. Moreover, this is also consistent with the fact that  $\Delta\Phi$  is not yet converged at a nominal coverage of 4 ML (actual 1.75 ML).

### Surface-molecule coupling

It is important to test our explanation of the interfacial electronic structure against alternative explanations. An important counter-hypothesis for the abrupt change in HOMO ionization energy might be strong coupling of the first molecular layer to the surface, which might give rise to new and different molecular features at the interface. Fortunately, the electronic structure of the oxidized surface contains ideal markers for assessing the nature of electronic coupling between the surface and the molecular film. Because oxygen atoms exist only in the surface reconstruction, electrons in bands with oxygen character are localized at the crystal surface,<sup>65</sup> and thus extremely sensitive to molecular adsorption, similar to Shockley surface states on coinage metal (111) surfaces.<sup>66,67</sup> Along  $\bar{\Gamma} - \bar{Y}$ , these bands disperse well beyond the bandwidth of the molecular DOS at similar energies,<sup>23,68-71</sup> allowing us to test molecular adsorption effects on band dispersion as an indicator of the extent of interfacial hybridization in the first molecular layer. Figure 5 gives the experimental band diagram for Cu(110)-(2x1)O along  $\bar{\Gamma} - \bar{Y}$ , with bands

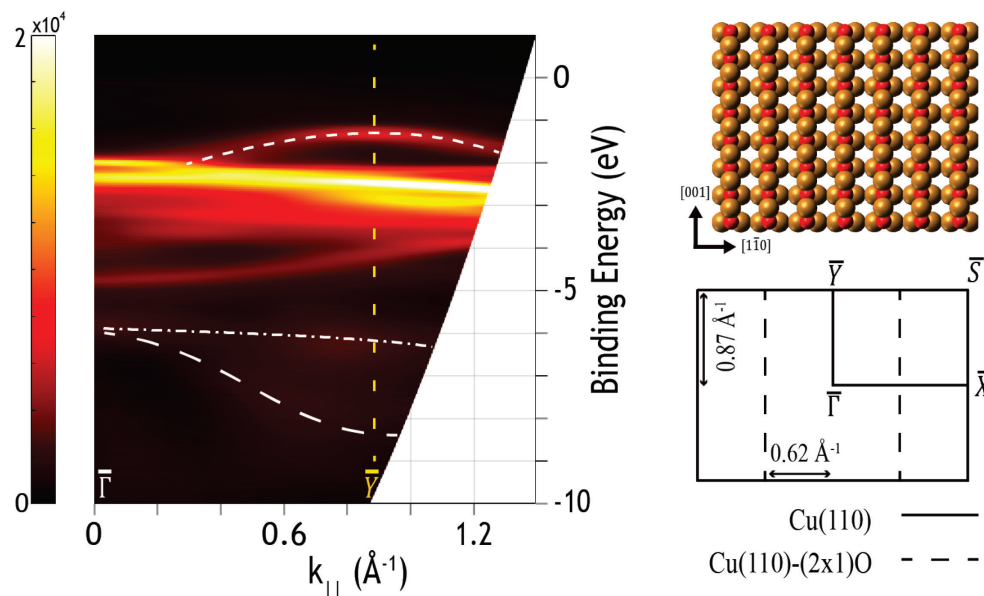


Figure 5. Background subtracted ARPES data for pristine Cu(110)-(2x1)O along  $\bar{\Gamma} - \bar{Y}$ . Bands with oxygen  $2p$  character are indicated by white dashed lines: short dash - antibonding  $2p_x$  and  $2p_z$ , dash dot - bonding  $2p_x$  and  $2p_z$ , long dash - bonding  $2p_y$ . Intense features between -2 and -5 eV are Cu(110) d-bands. Also shown is a cartoon of the Cu(110)-(2x1)O lattice and the respective Brillouin zone.

derived from oxygen  $2p$  orbitals indicated by white dashed lines. We note that neither the Cu(110) surface state nor the antibonding oxygen  $2p_y$  band are observed: The former shifts above  $E_F$  on the reconstructed surface, and the latter mixes strongly with bulk Cu states and cannot be distinguished any longer.<sup>65</sup>

Figure 6 shows how thin film growth of the first ML modifies these bands. From the 0.25 ML CuPc data (Figure 6a), we see that the presence of molecules barely affects the dispersion of the surface bands. Because CuPc forms ordered islands, the majority of the surface sampled by photoemission is still pristine Cu(110)-(2x1)O. At 0.5 ML CuPc, however, photoemission from the molecular film is significant enough to show a localization of the oxygen  $2p_y$ -derived band (long dash line in Figure 6b) due to hybridization with a nondispersive molecular feature at  $\sim$ -6 eV to -7 eV binding energy (see also Figure 1a). Yet, the dispersion of antibonding oxygen  $2p_x$ - and  $2p_z$ -derived bands, both closer to  $E_F$  than the O  $2p_y$  band, is unaltered. By 0.75 ML, the oxygen

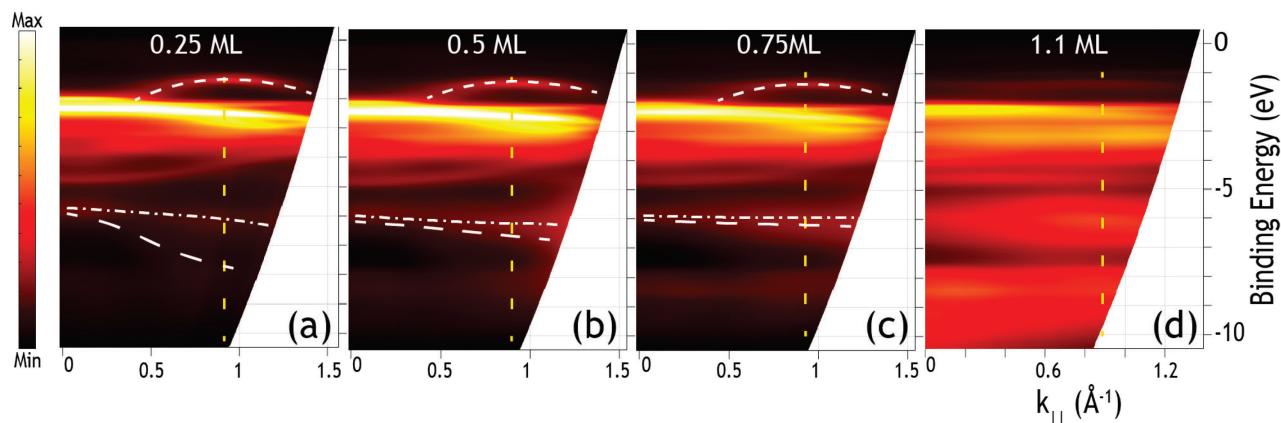


Figure 6. The effect of CuPc growth on the band structure of Cu(110)-(2x1)O. Bands with oxygen  $2p$  character are indicated as in Figure 5: short dash - antibonding  $2p_x$  and  $2p_z$ , dash dot - bonding  $2p_x$  and  $2p_z$ , long dash - bonding  $2p_y$ . The  $\bar{Y}$  point of the surface Brillouin zone is indicated with a yellow dashed line. (a) 0.25 ML CuPc. (b) 0.5 ML CuPc. (c) 0.75 ML CuPc. (d) 1.1 ML CuPc.

$2p_y$  band is completely localized and indistinguishable from the broad molecular feature, while the antibonding oxygen  $2p_x$ - and  $2p_z$ -derived bands are still clearly visible (Figure 6c) without exhibiting major changes to their dispersion. The angle-resolved data for 1.1 ML CuPc overwhelmingly project the non-dispersive molecular DOS (Figure 6d), but as can be seen more clearly in Figure 4, the antibonding oxygen  $2p_x$ - and  $2p_z$ -derived bands can still be observed upon close inspection, and they still disperse significantly. In contrast and at all coverages, the HOMO<sub>IL</sub> remains entirely localized. What little surface-molecule coupling does exist does not enhance intermolecular coupling to delocalize molecular features, in contrast to observations in strongly coupled and ordered interfaces of pentacene on Cu(110).<sup>72</sup>

The conclusion from the angle-resolved data must therefore be that while some hybridization is occurring between the surface and the molecules, especially in lower-lying orbitals, electronic coupling of CuPc frontier orbitals to the surface and creation of new interfacial states is quite minimal. Furthermore, the survival and dispersion of the antibonding surface bands also demonstrates that significant distortion of the surface lattice does not occur upon adsorption

of the molecule. These observations, together with the mobility of first layer molecules even at 5 K (evident from STM image noise in Figure 3a), allow us to conclude that the two different HOMO levels are *not* due to strong coupling of the molecules in the first layer followed by layer decoupling, and are instead the result of a structural transition in the film.

### Summary of interfacial energetics

To summarize our findings, an energy-level diagram is presented in Figure 7. We calculate ionization energies only from mostly complete layers to avoid complications due to local vacuum level variations in the presence of distributed island growth. Thus, molecules in the first full layer of CuPc on Cu(110)-(2x1)O adsorb flat on the surface with the HOMO<sub>IL</sub> centered at  $\sim -1.5$  eV below  $E_F$  (Figure 7a) to give an ionization energy of 6.05(7) eV, which is in line with reports of CuPc on other surfaces.<sup>73</sup> Initial growth of the second layer shows a HOMO<sub>Film</sub> binding

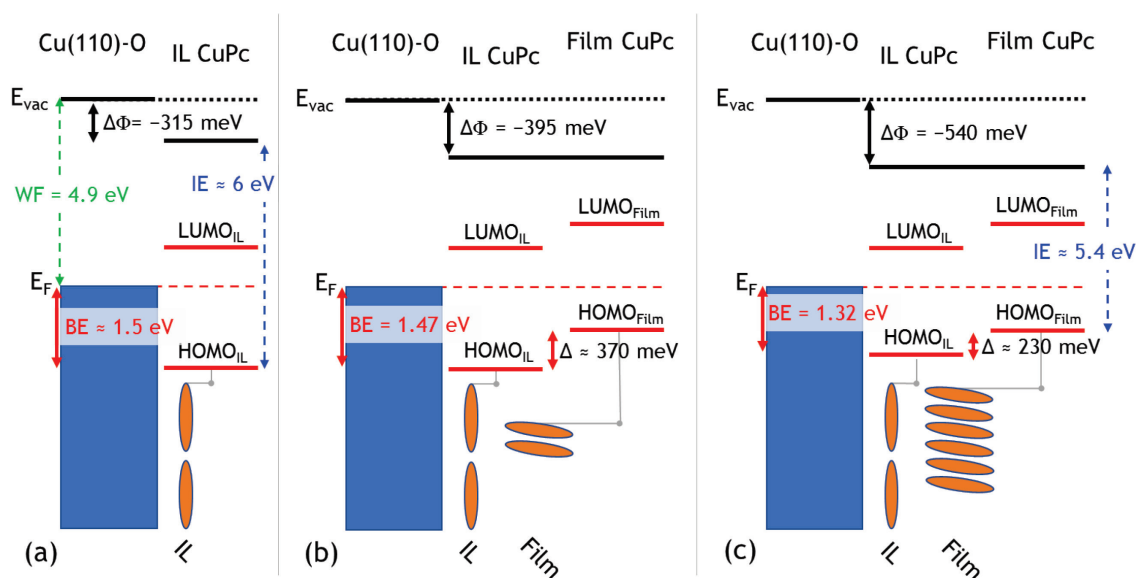


Figure 7. Energy-level diagram for the growth of CuPc on Cu(110)-(2x1)O. (a) 1 ML CuPc: Molecules lie flat on the surface in the interface (first) layer (IL). (b)  $\sim 1.25$  ML CuPc: Upon saturation of the IL, the next layer of molecules grows in a standing orientation. Due to the changing packing density, these coverages do not correspond to those in previous figures. (c)  $\sim 1.75$  ML CuPc: The nearly full second layer of standing molecules.

energy  $\sim 370$  meV lower than that of the HOMO<sub>IL</sub> (Figure 7b). The ionization energy for a molecule in a nearly full second layer is 5.43(7) eV (Figure 7a and 7c), a drop of over 0.6 eV from the interfacial layer. Such a dramatic change in ionization energy, accompanied by a work function difference  $\Delta\Delta\Phi$  of only -0.225 eV between the two films, can be understood by an abrupt transition to standing CuPc in the second layer. The magnitude of the change in ionization energy is comparable to that for the case of reorientation of sexithiophenes on Ag(111).<sup>18</sup> To our knowledge, this is the first time that such electronic and structural effects have been observed in room temperature-grown phthalocyanine films, and it enables us to offer a straightforward interpretation of the influence of different thin film phases on the interfacial electronic structure. Furthermore, we have demonstrated that surface modification by oxygen chemisorption is critical for ordered first layer growth, suppressing cooperative nanoribbon formation on the reactive Cu(110) surface. The interface layer templates the standing second layer and ultimately leads to the striking changes in electronic structure observed in the bilayer film.

## Conclusions

In conclusion, we observe a unique evolution of interfacial electronic structure for CuPc films on Cu(110)-(2x1)O, and show that this behavior is the result of an abrupt transition in film structure between the first and second layers. The presence of two different coverage-dependent thin film phases for a single organic / metal interface enable us to interpret changes to the interfacial electronic structure directly based on simple electrostatic arguments. Specifically, we show that oxygen chemisorption on the Cu(110) surface enables growth of an interface layer of ordered, flat-lying molecules which template a standing orientation for CuPc in the subsequent layer. The anisotropic charge distribution in CuPc drastically decreases the HOMO ionization energy for standing molecules, and the effect of this structural transition on interfacial energetics

is a 600 meV ionization energy drop between the interfacial layer and subsequent layers. The results of our findings have important implications for organic electronics:<sup>18</sup> Large energy-level offsets can be realized between two adjacent thin-film layers and with only one molecular species, two properties that are important for the miniaturization and functionality of electronic devices. In summary, we have shown that influencing interfacial interactions through a precisely controlled modification of the surface atomic structure is a simple and effective way to tailor the structural and electronic properties of organic semiconductor interfaces.

## References

- (1) Mazziro, K. A.; Luscombe, C. K. *Chem. Soc. Rev.* **2015**, *44*, 78–90.
- (2) Beaujuge, P. M.; Fréchet, J. M. J. *J. Am. Chem. Soc.* **2011**, *133*, 20009–20029.
- (3) Liao, C.; Yan, F. *Polym. Rev.* **2013**, *53*, 352–406.
- (4) Goiri, E.; Borghetti, P.; El-Sayed, A.; Ortega, J. E.; De Oteyza, D. G. *Adv. Mater.* **2016**, *28*, 1340–1368.
- (5) Egger, D. A.; Liu, Z.-F.; Neaton, J. B.; Kronik, L. *Nano Lett.* **2015**, *15*, 2448–2455.
- (6) Vázquez, H.; Dappe, Y. J.; Ortega, J.; Flores, F. *J. Chem. Phys.* **2007**, *126*, 144703.
- (7) Oehzelt, M.; Koch, N.; Heimel, G. *Nat. Commun.* **2014**, *5*, 4174.
- (8) Natan, A.; Kronik, L.; Haick, H.; Tung, R. T. *Adv. Mater.* **2007**, *19*, 4103–4117.
- (9) Liu, W.; Carrasco, J.; Santra, B.; Michaelides, A.; Scheffler, M.; Tkatchenko, A. *Phys. Rev. B - Condens. Matter Mater. Phys.* **2012**, *86*, 245405.
- (10) Monti, O. L. A. *J. Phys. Chem. Lett.* **2012**, *3*, 2342–2351.
- (11) Schöll, A.; Kilian, L.; Zou, Y.; Ziroff, J.; Hame, S.; Reinert, F.; Umbach, E.; Fink, R. H. *Science* **2010**, *329*, 303–305.
- (12) Wießner, M.; Hauschild, D.; Schöll, A.; Reinert, F.; Feyer, V.; Winkler, K.; Krömker, B. *Phys. Rev. B - Condens. Matter Mater. Phys.* **2012**, *86*, 45417.
- (13) Kilian, L.; Hauschild, A.; Temirov, R.; Soubatch, S.; Schöll, A.; Bendounan, A.; Reinert, F.; Lee, T. L.; Tautz, F. S.; Sokolowski, M.; et al. *Phys. Rev. Lett.* **2008**, *100*, 136103.
- (14) Hofmann, O. T.; Glowatzki, H.; Bürker, C.; Rangger, G. M.; Bröker, B.; Niederhausen, J.; Hosokai, T.; Salzmann, I.; Blum, R.-P.; Rieger, R.; et al. *J. Phys. Chem. C* **2017**, *121*, 24657–24668.
- (15) Willenbockel, M.; Lüftner, D.; Stadtmüller, B.; Koller, G.; Kumpf, C.; Soubatch, S.; Puschnig, P.; Ramsey, M. G.; Tautz, F. S. *Phys. Chem. Chem. Phys.* **2015**, *17*, 1530–1548.
- (16) Xiao, K.; Deng, W.; Keum, J. K.; Yoon, M.; Vlassiouk, I. V.; Kendal, W.; Li, A.; Kravchenko, I. I.; Gu, G.; Payzant, E. A.; et al. *JACS* **2013**, *135*, 3680–3687.
- (17) Hollerer, M.; Lüftner, D.; Hurdax, P.; Ules, T.; Soubatch, S.; Tautz, F. S.; Koller, G.; Puschnig, P.; Sterrer, M.; Ramsey, M. G. *ACS Nano* **2017**, *11*, 6252–6260.
- (18) Duhm, S.; Heimel, G.; Salzmann, I.; Glowatzki, H.; Johnson, R. L.; Vollmer, A.; Rabe, J. P.; Koch, N. *Nat. Mater.* **2008**, *7*, 326–332.

- (19) Takada, M.; Tada, H. *Chem. Phys. Lett.* **2004**, *392*, 265–269.
- (20) Maughan, B.; Zahl, P.; Sutter, P.; Monti, O. L. A. *J. Phys. Chem. C* **2015**, *119*, 27416–27425.
- (21) Kröger, I.; Stadtmüller, B.; Kumpf, C. *New J. Phys.* **2016**, *18*, 113022.
- (22) Zahl, P.; Wagner, T.; Möller, R.; Klust, A. *J. Vac. Sci. Technol. B* **2010**, *28*, C4E39–C4E47.
- (23) DiDio, R. A.; Zehner, D. M.; Plummer, E. W. *J. Vac. Sci. Technol. A* **1984**, *2*, 852–855.
- (24) Wendelken, J. F. *Surf. Sci.* **1981**, *108*, 605–616.
- (25) Zou, Y.; Kilian, L.; Schöll, A.; Schmidt, T.; Fink, R.; Umbach, E. *Surf. Sci.* **2006**, *600*, 1240–1251.
- (26) Maughan, B.; Zahl, P.; Sutter, P.; Monti, O. L. A. *Phys. Rev. B* **2017**, *96*, 235133.
- (27) Ilyas, N.; Monti, O. L. A. *Phys. Rev. B* **2014**, *90*, 125435.
- (28) Koch, N.; Kahn, A.; Ghijssen, J.; Pireaux, J. J.; Schwartz, J.; Johnson, R. L.; Elschner, A. *Appl. Phys. Lett.* **2003**, *82*, 70–72.
- (29) Heimel, G.; Romaner, L.; Zojer, E.; Bredas, J.-L. *Acc. Chem. Res.* **2008**, *41*, 721–729.
- (30) Tsiper, E. V.; Soos, Z. G.; Gao, W.; Kahn, A. *Chem. Phys. Lett.* **2002**, *360*, 47–52.
- (31) Fukagawa, H.; Yamane, H.; Kataoka, T.; Kera, S.; Nakamura, M.; Kudo, K.; Ueno, N. *Phys. Rev. B - Condens. Matter Mater. Phys.* **2006**, *73*, 24–26.
- (32) Gorgoi, M.; Zahn, D. R. T. *Org. Electron.* **2005**, *6*, 168–174.
- (33) Sugiyama, T.; Sasaki, T.; Kera, S.; Ueno, N.; Munakata, T. *Appl. Phys. Lett.* **2006**, *89*.
- (34) Peisert, H.; Knupfer, M.; Schwieger, T.; Auerhammer, J. M.; Golden, M. S.; Fink, J. J. *Appl. Phys.* **2002**, *91*, 4872–4878.
- (35) Sinha, S.; Mukherjee, M. *Appl. Surf. Sci.* **2015**, *353*, 540–547.
- (36) Kera, S.; Yabuuchi, Y.; Yamane, H.; Setoyama, H.; Okudaira, K. K.; Kahn, A.; Ueno, N. *Phys. Rev. B - Condens. Matter Mater. Phys.* **2004**, *70*, 1–6.
- (37) Menzli, S.; Laribi, A.; Mrezguia, H.; Arbi, I.; Akremi, A.; Chefi, C.; Chérioux, F.; Palmino, F. *Surf. Sci.* **2016**, *654*, 39–47.
- (38) Toader, M.; Shukryna, P.; Knupfer, M.; Zahn, D. R. T.; Hietschold, M. *Langmuir* **2012**, *28*, 13325–13330.
- (39) Petraki, F.; Peisert, H.; Aygül, U.; Latteyer, F.; Uihlein, J.; Vollmer, A.; Chassé, T. *J. Phys. Chem. C* **2012**, *116*, 11110–11116.
- (40) Evangelista, F.; Ruocco, A.; Gotter, R.; Cossaro, A.; Floreano, L.; Morgante, A.; Crispoldi, F.; Betti, M. G.; Mariani, C. *J. Chem. Phys.* **2009**, *131*.
- (41) Salaneck, W. R. *Phys. Rev. Lett.* **1978**, *40*, 60–63.
- (42) Terentjevs, A.; Steele, M. P.; Blumenfeld, M. L.; Ilyas, N.; Kelly, L. L.; Fabiano, E.; Monti, O. L. A.; Della Sala, F. *J. Phys. Chem. C* **2011**, *115*, 21128–21138.
- (43) Ilyas, N.; Kelly, L. L.; Monti, O. L. A. *Mol. Phys.* **2013**, *111*, 2175–2188.
- (44) Steele, M. P.; Blumenfeld, M. L.; Monti, O. L. A. *J. Chem. Phys.* **2010**, *133*, 124701.
- (45) Blumenfeld, M. L.; Steele, M. P.; Ilyas, N.; Monti, O. L. A. *Surf. Sci.* **2010**, *604*, 1649–1657.
- (46) Giovanelli, L.; Amsalem, P.; Angot, T.; Petaccia, L.; Gorovikov, S.; Porte, L.; Goldoni, A.; Themlin, J. M. *Phys. Rev. B - Condens. Matter Mater. Phys.* **2010**, *82*, 125431.
- (47) Hill, I. G.; Mäkinen, A. J.; Kafafi, Z. H. *J. Appl. Phys.* **2000**, *88*, 889–895.
- (48) Tao, Y.; Mao, H.; He, P. *J. Appl. Phys.* **2015**, *117*.
- (49) Ryno, S. M.; Risko, C.; Brédas, J. L. *ACS Appl. Mater. Interfaces* **2016**, *8*, 14053–14062.
- (50) Huang, H.; Chen, W.; Wee, A. T. S. *J. Phys. Chem. C* **2008**, *112*, 14913–14918.

- (51) Hooks, D. E.; Fritz, T.; Ward, M. D. *Adv. Mater.* **2001**, *13*, 227–241.
- (52) Abadía, M.; González-Moreno, R.; Sarasola, A.; Otero-Irurueta, G.; Verdini, A.; Floreano, L.; Garcia-Lekue, A.; Rogero, C. *J. Phys. Chem. C* **2014**, *118*, 29704–29712.
- (53) Jensen, F.; Besenbacher, F.; Laegsgaard, E.; Stensgaard, I. *Phys. Rev. B* **1990**, *41*, 10233–10236.
- (54) Besenbacher, F.; Nørskov, J. K. *Prog. Surf. Sci.* **1993**, *44*, 5–66.
- (55) Chiang, C.; Xu, C.; Han, Z.; Ho, W. *Science* **2014**, *344*, 885–888.
- (56) Wang, C.; Liu, X.; Wang, C.; Xu, X.; Li, Y.; Xie, F.; Gao, Y. *Appl. Phys. Lett.* **2015**, *106*, 2–6.
- (57) Biswas, I.; Peisert, H.; Nagel, M.; Casu, M. B.; Schuppler, S.; Nagel, P.; Pellegrin, E.; Chassé, T. *J. Chem. Phys.* **2007**, *126*.
- (58) Blumenfeld, M. L.; Steele, M. P.; Monti, O. L. A. *J. Phys. Chem. Lett.* **2010**, *1*, 145–148.
- (59) Salzmann, I.; Duhm, S.; Heimel, G.; Oehzelt, M.; Johnson, R. L.; Rabe, J. P.; Koch, N. *J. Am. Chem. Soc.* **2008**, *130*, 12870–12871.
- (60) Duhm, S.; Salzmann, I.; Heimel, G.; Oehzelt, M.; Haase, A.; Johnson, R. L.; Rabe, J. P.; Koch, N. *Appl. Phys. Lett.* **2009**, *94*, 1–4.
- (61) Hasegawa, S.; Tanaka, S.; Yamashita, Y.; Inokuchi, H.; Fujimoto, H.; Kamiya, K.; Seki, K.; Ueno, N. *Phys. Rev. B* **1993**, *48*, 2596–2600.
- (62) Berge, K.; Goldmann, a. *Surf. Sci.* **2003**, *540*, 97–106.
- (63) Gould, R. D. *Coord. Chem. Rev.* **1996**, *156*, 237–274.
- (64) Chen, X.; Fu, Y. S.; Ji, S. H.; Zhang, T.; Cheng, P.; Ma, X. C.; Zou, X. L.; Duan, W. H.; Jia, J. F.; Xue, Q. K. *Phys. Rev. Lett.* **2008**, *101*, 1–4.
- (65) Cabrera-Sanfeliix, P.; Lin, C.; Arnau, A.; Sánchez-Portal, D. *J. Physics: Condens. Matter* **2013**, *25*, 135003.
- (66) Schwalb, C. H.; Sachs, S.; Marks, M.; Schöll, A.; Reinert, F.; Umbach, E.; Höfer, U. *Phys. Rev. Lett.* **2008**, *101*, 146801.
- (67) Caplins, B. W.; Suich, D. E.; Shearer, A. J.; Harris, C. B. *J. Phys. Chem. Lett.* **2014**, *5*, 1679–1684.
- (68) Courths, R.; Hüfner, S.; Kemkes, P.; Wiesen, G. *Surf. Sci.* **1997**, *376*, 43–59.
- (69) Pforte, F.; Gerlach, a.; Goldmann, a.; Matzdorf, R.; Braun, J.; Postnikov, a. *Phys. Rev. B* **2001**, *63*, 165405.
- (70) Ozawa, R.; Yamane, A.; Morikawa, K.; Ohwada, M.; Suzuki, K.; Fukutani, H. *Surf. Sci.* **1996**, *346*, 237–242.
- (71) Matzdorf, R.; Goldmann, A. *Surf. Sci.* **1998**, *413*, 61–68.
- (72) Yamane, H.; Yoshimura, D.; Kawabe, E.; Sumii, R.; Kanai, K.; Ouchi, Y.; Ueno, N.; Seki, K. *Phys. Rev. B* **2007**, *76*.
- (73) Ellis, T. S.; Park, K. T.; Hulbert, S. L.; Ulrich, M. D.; Rowe, J. E. *J. Appl. Phys.* **2004**, *95*, 982–988.